49th AIAA Aerospace Sciences Meeting including the New Horizons Forum and Aerospace Exposition
4 - 7 January 2011, Orlando, Florida
AIAA 2011-365

Development and validation of a high-order shock-fitting non-equilibrium flow solver

Xiaowen Wang* and Xiaolin Zhong #1
Mechanical and Aerospace Engineering Department
University of California, Los Angeles, CA 90095

Abstract

Many important scientific and engineering applications, such as strong shock and turbulence interactions and hypersonic boundary-layer stability and transition, involve strong shocks. These processes are strongly nonlinear and proven to be very complex to understand with existing tools. The most widely used shock capturing methods may incur numerical oscillations near the shock and may not be accurate enough for numerical simulations of hypersonic boundary-layer stability and transition problems. Furthermore, effects of internal energy excitations, translation-vibration energy relaxation, ionizations, and chemical reactions among different species need to be considered, because gas temperature increases dramatically after strong shocks. To solve such problems, a unique approach of using high-order shock-fitting method is adopted, where the main shock is treated by shock-fitting method as a sharp boundary. The code is validated by comparisons with experimental datasets and numerical simulation results obtained from open literature.

1. Introduction

Hypersonic flow is categorized by certain physical phenomena that do not typically play an important role in subsonic and supersonic flows. These effects could be thin shock layers, entropy layers, viscous-inviscid interactions due to the high displacement thickness of boundary layers, and high temperature gas effects [1]. All these effects need to be considered for scientific and engineering applications involving strong shocks, such as strong shock and turbulence interactions [2-4] and hypersonic boundary-layer stability and transition [5-7].

At temperatures less then 500-800K, gas flow stays calorically perfect. Only translational and rotational energy modes are fully excited while the excitations of vibration energy mode and chemical reactions are negligible, as a result specific heat capacities remain constant. For temperatures around 800-2000K, vibration energy mode takes an important role in sharing the total energy with the translational and rotational modes. Near the lower temperature limit of this regime, translation-vibration energy relaxation between harmonic oscillator molecules dominates because most of the molecules are near the ground vibrational state. Near the higher limit of this regime, vibration-vibration energy relaxation becomes significantly active because not only are vibrationally excited molecules highly populated but also vibration-vibration energy relaxation is considerably

* Research Associate, Mechanical and Aerospace Engineering Department, UCLA, AIAA Senior Member
# Professor, Mechanical and Aerospace Engineering Department, UCLA, AIAA Associate Fellow

faster than its translation-vibration counter-part. Also, the vibrational oscillation becomes inharmonic as the temperature approaches the dissociation level. However, results within the harmonic oscillator approximation are known to be sufficiently accurate enough for most practical purposes [8]. For temperatures above 2000-2500K, vibration energy mode is fully excited and O2 starts dissociating. Around 4000K, O2 is completely dissociated and N2 starts dissociating. When the temperature reaches 9000k, most of the N2 is dissociated. Coincidentally, this is the temperature around which the both dissociated N and O atoms become ionized. Around 12000K, all the gases are completely dissociated and about 14% of them are ionized such that there is a sufficient amount of free charges, enough to make electromagnetic forces. Radiation emitted and absorbed by the gas can become important and could eventually modify the energy distribution in the flow field. At 20000K, double dissociation begins. And finally when it reaches 30000K, the gas is completely ionized [9]. These regimes correspond to M_∞ greater or much greater than 30.

All the high temperature gas effects are due to molecular collisions which occur at finite rates. When the collision rates are much faster than flow rates, it is called as “equilibrium flow”. On the other hand, if the collision rates are much slower than flow rates, it is called as “frozen flow”. Unfortunately, neither of these two situations can completely describe the hypersonic flow over a space/air vehicle. There will always be regions where the collision rates are in the same vicinity of the flow rates, moreover different species will have different reaction rates and different energy relaxation rates. Therefore, energy transfers between bulk kinetic energy, translational energies, chemical energies, and vibration energies of different species are actively in progress at many locations in a hypersonic thermochemical non-equilibrium flow. When these effects start to play dominant roles, the flow is called “non-equilibrium flow”.

In the past years, interest in various types of vehicles in hypersonic flow regime produced numerous structured grid based non-equilibrium flow solvers. According to recent publications, Laura, DPLR, and Lore are the most frequently referenced and are intensively validated against each other [10] and also against wind tunnel tests. LAURA (Langley Aerothermodynamic Upwind Relaxation Algorithm) is mainly developed by Peter Gnoffo at the NASA Langley Research Center [11-14]. It uses Roe's flux difference splitting scheme with Yee's second-order symmetric total variation diminishing scheme to model the inviscid fluxes. Steady state solution is obtained using either point or line relaxation time integration scheme. The vibration energy mode is assumed to be in equilibrium with the electronic energy, and translational energy is assumed to be in equilibrium with the rotational energy mode. The code supports multi-block structured grids and MPI communication for massive parallel computing. DPLR (Data-Parallel Line Relaxation) is initially developed at University of Minnesota by Wright, Candler, and Bose [15]. This is further developed at NASA Ames research center [10]. DPLR implicit method is optimized for efficient parallel computing by arranging the body normal dependent data with local CPU in order to perform the relaxation process simultaneously in parallel mode. DPLR uses third order modified Steger-Warming flux splitting scheme with MUSCL data reconstruction to model the inviscid fluxes. Unlike LAURA, the vibration energy mode is separately treated from the electronic energy modes, and translational energy is assumed to be equilibrium with the rotational and electronic

energy mode. It also supports multi-block structured grids. Lore [16] was developed at the Advanced Operations and Engineering Services Group in Europe. The flow solver uses modified AUSM scheme with MUSCL data reconstruction to achieve second-order accuracy coupled with a van Albada limiter. Time advancement to a steady-state solution is achieved using an alternating direction line Gauss-Seidel implicit relaxation method. The code supports multi-block structured grids. This code covers a wide range of flight regimes from subsonic to hypersonic.

However, the most widely used shock capturing methods may incur numerical oscillations near the shock and may not be accurate enough for numerical simulations of hypersonic boundary-layer stability and transition problems. To solve problems including strong shocks and thermochemical non-equilibrium phenomena, we propose a unique approach of using high-order shock-fitting method. The main shock is treated by shock-fitting method as a sharp boundary. The shock dynamics is governed by shock jump conditions so that the interaction of the main shock with freestream disturbance is computed accurately. The main advantage of shock-fitting method is uniform high-order accuracy for flow containing shock waves and no spurious oscillations near the shock. On the contrary, most of the popular shock-capturing methods are only first-order accurate at the shock and may incur spurious numerical oscillations near the shock. The code is implemented based on a two-temperature model. It is assumed that translational and rotational energy modes are in equilibrium at translational temperature whereas vibration energy, electronic energy, and free electron energy are in equilibrium at vibration temperature. The flow solver uses fifth-order shock-fitting method of Zhong [17] with local Lax-Friedrichs flux splitting. In the computer code, both 5-species and 11-species chemistry sets of air are implemented. For convenience, governing equations and models of thermal properties and chemical reactions in this paper are all based on 11-species air. They can be applied to 5-species air straightforward. The code has been tested on a number of non-equilibrium reacting flows.

2. Governing equations

2.1 Governing equations

For thermochemical non-equilibrium flows, it is assumed that free electron has the same average velocity as that of heavy particles so that there is zero conduction current in the flow. It is also assumed that electron number density equals to ion number density so that there is no charge separation in flow. The governing equations are Navier-Stokes equation with source terms. For the 11-species chemistry of air, they consist of the flowing equations.

$$\frac{\partial \rho_s}{\partial t} + \frac{\partial}{\partial x_j}(\rho_s u_j) - \frac{\partial}{\partial x_j}(\rho D_s \frac{\partial y_s}{\partial x_j}) = \omega_s \tag{1}$$

$$\frac{\partial}{\partial t}(\rho u_i) + \frac{\partial}{\partial x_j}(\rho u_i u_j + p\delta_{ij}) - \frac{\partial}{\partial x_j}\left[\mu\left(\frac{\partial u_i}{\partial x_j} + \frac{\partial u_j}{\partial x_i}\right) - \frac{2}{3}\mu\frac{\partial u_k}{\partial x_k}\delta_{ij}\right] = 0 \tag{2}$$

$$\frac{\partial \rho E}{\partial t}+\frac{\partial}{\partial x_j}(\rho H u_j)-\frac{\partial}{\partial x_j}\left[u_i\mu\left(\frac{\partial u_i}{\partial x_j}+\frac{\partial u_j}{\partial x_i}\right)-\frac{2}{3}u_i\mu\frac{\partial u_k}{\partial x_k}\delta_{ij}\right]$$
$$-\frac{\partial}{\partial x_j}\left(\rho\sum_{s=1}^{11}h_s D_s\frac{\partial y_s}{\partial x_j}\right)-\frac{\partial}{\partial x_j}\left(K\frac{\partial T}{\partial x_j}+K_V\frac{\partial T_V}{\partial x_j}\right)=0 \qquad (3)$$

$$\frac{\partial \rho e_V}{\partial t}+\frac{\partial}{\partial x_j}(\rho e_V u_j)-\frac{\partial}{\partial x_j}(\rho\sum_{s=1}^{11}h_{V,s}D_s\frac{\partial y_s}{\partial x_j})-\frac{\partial}{\partial x_j}\left(K_V\frac{\partial T_V}{\partial x_j}\right)$$
$$=-p_e\frac{\partial u_j}{\partial x_j}+3\rho_e R(T-Tv)\sum_{s=1}^{10}\frac{\upsilon_{es}}{M_s}-\sum_{s=6}^{10}\dot{n}_{e,s}\hat{I}_s$$
$$+\sum_{s=1}^{3}(Q_{T-V,s}+\omega_s e_{V,s})+\sum_{s=6}^{8}(Q_{T-V,s}+\omega_s e_{V,s}) \qquad (4)$$

where,

$$y_s=\frac{(\rho_s/M_s)}{\sum_{i=1}^{11}(\rho_i/M_i)} \qquad \rho=\sum_{s=1}^{n}\rho_s \qquad p=\sum_{s=1}^{11}p_s=\sum_{s=1}^{11}\frac{\rho_s\bar{R}T}{M_s}$$

$$E=\frac{u_i u_i}{2}+\sum_{s=1}^{11}\frac{\rho_s e_s}{\rho} \qquad H=E+\frac{p}{\rho} \qquad h_{V,s}=\begin{cases}e_{V,s} & (s\neq e)\\ e_{V,e}+\dfrac{\bar{R}T_V}{M_e}\end{cases}$$

$\bar{R}$ is the universal gas constant. The governing equations for 5-species chemistry of air are quite similar except that the first three terms on right hand side of the vibration energy equation (4) are neglected. In this paper, the 11-species of air is defined as in Table 1.

Table 1. index of the 11-species of air

index	1	2	3	4	5	6	7	8	9	10	11
species	N_2	O_2	NO	N	O	N_2+	O_2+	NO+	N+	O+	E

2.2 Governing equations in matrix form

For computer code implementation, the matrix form of governing equations is generally more convenient and straightforward. The corresponding matrix form of governing equations is as follows,

$$\frac{\partial U}{\partial t}+\frac{\partial F_1}{\partial x}+\frac{\partial F_2}{\partial y}+\frac{\partial F_3}{\partial z}+\frac{\partial G_1}{\partial x}+\frac{\partial G_2}{\partial y}+\frac{\partial G_3}{\partial z}=S \qquad (5)$$

Where F stands for inviscid flux,
G stands for viscous flux,
S stands for source terms.

$$U=\left(\rho_1,\rho_2,\rho_3,\cdots,\rho_{11},\rho u,\rho v,\rho w,\rho E,\rho e_V\right)^{\mathrm{T}}$$

The corresponding inviscid and viscous fluxes are as follows,

$$F_j = \begin{pmatrix} \rho_1 u_j \\ \rho_2 u_j \\ \rho_3 u_j \\ \vdots \\ \rho_{11} u_j \\ \rho u u_j + p\delta_{1j} \\ \rho v u_j + p\delta_{2j} \\ \rho w u_j + p\delta_{3j} \\ \rho H u_j \\ \rho e_V u_j \end{pmatrix} \quad G_j = \begin{pmatrix} \rho_1 v_{1j} \\ \rho_2 v_{2j} \\ \rho_3 v_{3j} \\ \vdots \\ \rho_{11} v_{11j} \\ -\tau_{1j} \\ -\tau_{2j} \\ -\tau_{3j} \\ -u_i\tau_{ij} + q_j + q_{Vj} + \sum_{s=1}^{5} \rho_s h_s v_{sj} \\ q_{Vj} + \sum_{s=1}^{3} \rho_s e_{V,s} v_{sj} \end{pmatrix} \quad S = \begin{pmatrix} \omega_1 \\ \omega_2 \\ \omega_3 \\ \vdots \\ \omega_{11} \\ 0 \\ 0 \\ 0 \\ 0 \\ \sum_{s=1}^{3} (Q_{T-V,s} + \omega_s e_{V,s}) \end{pmatrix}$$

In above equations, $v_{sj} = u_{sj} - u_j$ is diffusion velocity of species s.

2.3 Coordinate transform

The flow solver uses structured grids. Therefore, the following grid transform is applied.

$$\begin{cases} x = x(\xi,\eta,\zeta,\tau) \\ y = y(\xi,\eta,\zeta,\tau) \\ z = z(\xi,\eta,\zeta,\tau) \\ t = \tau \end{cases} \Leftrightarrow \begin{cases} \xi = \xi(x,y,z,t) \\ \eta = \eta(x,y,z,t) \\ \zeta = \zeta(x,y,z,t) \\ \tau = t \end{cases} \tag{6}$$

Jacobian of the transform,

$$J = \begin{vmatrix} x_\xi & y_\xi & z_\xi & 0 \\ x_\eta & y_\eta & z_\eta & 0 \\ x_\zeta & y_\zeta & z_\zeta & 0 \\ x_\tau & y_\tau & z_\tau & 1 \end{vmatrix} \tag{7}$$

With the transform relation, the governing equations in (ξ,η,ζ,τ) coordinate system are written as

$$\frac{\partial(JU)}{\partial\tau} + \frac{\partial\tilde{F}_1}{\partial\xi} + \frac{\partial\tilde{F}_2}{\partial\eta} + \frac{\partial\tilde{F}_3}{\partial\zeta} + \frac{\partial\tilde{G}_1}{\partial\xi} + \frac{\partial\tilde{G}_2}{\partial\eta} + \frac{\partial\tilde{G}_3}{\partial\zeta} = JS \tag{8}$$

Where

$$\tilde{F}_1 = J\xi_x F_1 + J\xi_y F_2 + J\xi_z F_3 + JU\xi_t$$
$$\tilde{F}_2 = J\eta_x F_1 + J\eta_y F_2 + J\eta_z F_3 + JU\eta_t$$
$$\tilde{F}_3 = J\zeta_x F_1 + J\zeta_y F_2 + J\zeta_z F_3 + JU\zeta_t$$
$$\tilde{G}_1 = J\xi_x G_1 + J\xi_y G_2 + J\xi_z G_3$$

$$\tilde{G}_2 = J\eta_x G_1 + J\eta_y G_2 + J\eta_z G_3$$
$$\tilde{G}_3 = J\zeta_x G_1 + J\zeta_y G_2 + J\zeta_z G_3$$

3. Numerical method

The governing equations are solved by the fifth-order shock-fitting method of Zhong [17]. For the thermally non-equilibrium and chemically reacting system (5) in the direction, $\mathrm{k} = (k_1, k_2, k_3)$, the corresponding inviscid flux term is

$$\mathrm{F} = \begin{pmatrix} \rho_1 \mathrm{k}\,\mathrm{u} \\ \rho_2 \mathrm{k}\,\mathrm{u} \\ \rho_3 \mathrm{k}\,\mathrm{u} \\ \vdots \\ \rho_{11} \mathrm{k}\,\mathrm{u} \\ \rho u \mathrm{k}\,\mathrm{u} + p k_1 \\ \rho v \mathrm{k}\,\mathrm{u} + p k_2 \\ \rho w \mathrm{k}\,\mathrm{u} + p k_3 \\ \rho H \mathrm{k}\,\mathrm{u} \\ \rho e_V \mathrm{k}\,\mathrm{u} \end{pmatrix} \tag{9}$$

Hence the Jacobian of flux is defined as,

$$\mathrm{A} = \frac{\partial \mathrm{F}}{\partial \mathrm{U}} = L\Lambda R \tag{10}$$

$$A = |\mathrm{k}| \begin{bmatrix} \tilde{U}(\delta_{sr} - c_s) & c_s n_x & c_s n_y & c_s n_z & 0 & 0 \\ \tilde{\gamma}_r n_x - \tilde{U}u & -\beta u n_x + u n_x + \tilde{U} & -\beta v n_x + u n_y & -\beta w n_x + u n_z & \beta n_x & \phi n_x \\ \tilde{\gamma}_r n_y - \tilde{U}v & -\beta u n_y + v n_x & -\beta v n_y + v n_y + \tilde{U} & -\beta w n_y + v n_z & \beta n_y & \phi n_y \\ \tilde{\gamma}_r n_z - \tilde{U}w & -\beta u n_z + w n_x & -\beta v n_z + w n_y & -\beta w n_z + w n_z + \tilde{U} & \beta n_z & \phi n_z \\ \tilde{\gamma}_r \tilde{U} - \tilde{U}H & -\beta u \tilde{U} + H n_x & -\beta v \tilde{U} + H n_y & -\beta w \tilde{U} + H n_z & \beta \tilde{U} + \tilde{U} & \phi \tilde{U} \\ -\tilde{U} e_V & e_V n_x & e_V n_y & e_V n_z & 0 & \tilde{U} \end{bmatrix}$$

$$R = \begin{bmatrix} a^2 \delta_{sr} - c_s \tilde{\gamma}_r & \beta u c_s & \beta v c_s & \beta w c_s & -\beta c_s & -\phi c_s \\ -\tilde{V} & l_x & l_y & l_z & 0 & 0 \\ -\tilde{W} & m_x & m_y & m_z & 0 & 0 \\ \tilde{\gamma}_r - \tilde{U}a & a n_x - \beta u & a n_y - \beta v & a n_z - \beta w & \beta & \phi \\ \tilde{\gamma}_r + \tilde{U}a & -a n_x - \beta u & -a n_y - \beta v & -a n_z - \beta w & \beta & \phi \\ -e_V \tilde{\gamma}_r & \beta u e_V & \beta v e_V & \beta w e_V & -\beta e_V & a^2 - \phi e_V \end{bmatrix}$$

$$L=\begin{bmatrix} \delta_{sr}/a^2 & 0 & 0 & c_s/2a^2 & c_s/2a^2 & 0 \\ u/a^2 & l_x & m_x & (u+an_x)/2a^2 & (u-an_x)/2a^2 & 0 \\ v/a^2 & l_y & m_y & (v+an_y)/2a^2 & (v-an_y)/2a^2 & 0 \\ w/a^2 & l_z & m_z & (w+an_z)/2a^2 & (w-an_z)/2a^2 & 0 \\ \left[\beta(u^2+v^2+w^2)-\tilde{\gamma}_r\right]/\beta a^2 & \tilde{V} & \tilde{W} & (H+a\tilde{U})/2a^2 & (H-a\tilde{U})/2a^2 & -\phi/\beta a^2 \\ 0 & 0 & 0 & e_V/2a^2 & e_V/2a^2 & 1/a^2 \end{bmatrix}$$

The eigenvalues of Jacobian matrix (10) are

$$\lambda_{1,2,3,4,5,6,7,10}=|\mathrm{k}|\tilde{U} \tag{11}$$

$$\lambda_8=|\mathrm{k}|(\tilde{U}+a) \tag{12}$$

$$\lambda_9=|\mathrm{k}|(\tilde{U}-a) \tag{13}$$

where subscript "s" refers to row s and species s, whereas subscript "r" refers to column r and species r. Both s and r vary from 1 to 5 in the present model. The unit vector n is defined from vector k as

$$\mathrm{n}=(n_x,n_y,n_z)=\frac{(k_1,k_2,k_3)}{|\mathrm{k}|}$$

$\mathrm{l}=\left(l_x,l_y,l_z\right)$ and $\mathrm{m}=\left(m_x,m_y,m_z\right)$ are two unit vectors such that n , l , and m are mutually orthogonal.

$$\tilde{U}=un_x+vn_y+wn_z$$
$$\tilde{V}=ul_x+vl_y+wl_z$$
$$\tilde{W}=um_x+vm_y+wm_z$$

The derivative of pressure respecting to conservative variables comes from

$$dp=\beta(d\rho E-ud\rho u-vd\rho v-wd\rho w)+\phi d\rho e_V+\tilde{\gamma}_s d\rho_s \tag{14}$$

Where

$$\beta=\frac{\bar{R}}{\rho\sum_s c_s c_{v,tr}^s}\sum_{r=1}^{10}\frac{\rho_r}{M_r} \tag{15}$$

$$\phi=\frac{\bar{R}}{\rho C_{v,V}}\frac{\rho_e}{M_e}-\beta \tag{16}$$

$$\tilde{\gamma}_s=\frac{\bar{R}T_q}{M_s}+\beta\frac{u^2+v^2+w^2}{2}-\beta e_s-\phi e_{V,s} \tag{17}$$

$$a^2 = \sum_{s=1}^{11} c_s \tilde{\gamma}_s + \beta\left[H - (u^2 + v^2 + w^2)\right] + \phi e_V = (1+\beta)\frac{p}{\rho} \tag{18}$$

In equation (17), $T_q = T_V$ when s is an electron, otherwise, $T_q = T$.

The inviscid flux terms are discretized by a fifth-order upwind scheme, and the viscous flux terms are discretized by a sixth-order central scheme. For the inviscid flux vectors, a simple local Lax-Friedrichs scheme is used to split vectors into negative and positive wave fields. The conditions behind the shock are calculated using Rankine-Hugoniot relations across the shock, a compatibility relation from behind the shock, and the same species concentration across the shock. More details of the shock-fitting algorithm are included in Zhong's paper [17].

4. Nonequilibrium models

4.1 Models of vibration and electron energy

Three models of vibration and electron energy are implemented in the code. In Candler's thesis [18] and Hash et al.'s paper [14], vibration energy and electron energy are considered separately with different formula. While in Gnoffo et al.'s report [19] and McBride & Gordon's report [20], vibration and electron energy are calculated together from the curve fits of experimental correlations. The difference between these three models comes from how they evaluate specific total enthalpy of species and specific heat in constant pressure of species.

In Candler's thesis and Hash et al.'s paper, specific total enthalpy of species and specific heat in constant pressure of species are defined as,

$$h_s = c_{vs}T + \frac{p_s}{\rho_s} + E_V + h_s^0 \tag{19}$$

$$c_p^s = c_v^s + \frac{\bar{R}}{M_s} + c_V^s \tag{20}$$

where h_s^0 is the generation enthalpy of species. The variables on the right hand side of equations (19) and (20) are calculated from the following formula,

$$E_V = e_v + e_{els} \qquad c_v^s = c_{vtr,s} + c_{vrot,s} \qquad c_{vtr,s} = \frac{3\bar{R}}{2M_s}$$

$$c_{vrot,s} = \begin{cases} \dfrac{\bar{R}}{M_s} & (s = 1,3) \\ 0 & (otherwise) \end{cases} \qquad c_V^s = \frac{dE_V}{dT_V}$$

The related parameters for the 5-species air are listed in Table 2, obtained from Candler's thesis. The more complex model of electronic energy is obtained from Hash's paper.

Table 2. Parameters used in Candler's thesis

Species	h_s^0 (J/kg)	M_s (g)	θ_{vs} (K)	θ_{els} (K)	g_0	g_1
N2	0	28	3395	-	-	-
O2	0	32	2239	11341	3	2
NO	2.996123e6	30	2817	-	-	-
N	3.362161e7	14	-	27665	9	10
O	1.543119e7	16	-	22831	9	5

In Gnoffo et al.'s report, specific total enthalpy of species and specific heat in constant pressure of species are defined as,

$$h_s\left(T,T_V\right)=(c_{p,t}^s+c_{p,r}^s)(T-T_V)+h_s\left(T_V\right) \tag{21}$$

$$c_p^s\left(T\right)=\frac{\bar{R}}{M_s}\sum_{k=1}^{5}A_k^sT^{k-1} \tag{22}$$

where $h_s(T_V)=\frac{\bar{R}}{M_s}\left(\sum_{k=1}^{5}\frac{A_k^sT_V^k}{k}+A_6^s\right)$.

Parameters of the curve fit for 5-species air are listed in Table 3. With the temperature increasing from 300 K to 35000 K, five sets of curve fits are employed,

1. $300 \le T \le 1000$ 2. $1000 \le T \le 6000$ 3. $6000 \le T \le 15000$
4. $15000 \le T \le 25000$ 5. $25000 \le T \le 35000$

Table 3. curve fit parameters in Gnoffo et al.'s report

Species	Range	A_1	A_2	A_3	A_4	A_5	A_6
N2	1	3.674826	-1.208150e-3	2.324010e-6	- 6.321755e-10	- 2.257725e-13	- 1061.16
	2	2.896319	1.515486e-3	- 5.723527e-7	9.980739e-11	- 6.522355e-15	- 905.862
	3	3.727	4.684e-4	- 1.140e-7	1.154e-11	- 3.293e-16	- 1043.00
	4	9.637690	- 2.572840e-3	3.301980e-7	- 1.431490e-11	2.033260e-16	- 1043.00
	5	- 5.168080	2.333690e-3	- 1.295340e-7	2.787210e-12	- 2.135960e-17	- 1043.00
O2	1	3.625598	- 1.878218e-3	7.055454e-6	- 6.763513e-9	2.155599e-12	- 1047.52
	2	3.621953	7.361826e-4	- 1.965222e-7	3.620155e-11	- 2.894562e-15	- 1201.98
	3	3.721	4.254e-4	- 2.835e-8	6.050e-13	- 5.186e-18	- 1044.00
	4	3.486660	5.238420e-4	- 3.912340e-8	1.009350e-12	- 8.871830e-18	- 1044.00
	5	3.961980	3.944550e-4	- 2.950580e-8	7.397450e-13	- 6.420930e-18	- 1044.00
NO	1	4.045952	- 3.418178e-3	7.981919e-6	- 6.113931e-9	1.591907e-12	9745.39
	2	3.189	1.338228e-3	- 5.289932e-7	9.591933e-11	- 6.484793e-15	9828.33
	3	3.845	2.521e-4	- 2.658e-8	2.162e-12	- 6.381e-17	9764.00
	4	4.330870	- 5.808630e-5	2.805950e-8	- 1.569410e-12	2.410390e-17	9764.00
	5	2.350750	5.864300e-4	- 3.131650e-8	6.049510e-13	- 4.055670e-18	9764.00
N	1	2.503071	- 2.180018e-5	5.420528e-8	- 5.647560e-11	2.099904e-14	56098.9
	2	2.450268	1.066145e-4	- 7.465337e-8	1.879652e-11	- 1.025983e-15	56116.0
	3	2.748	- 3.909e-4	1.338e-7	- 1.191e-11	3.369e-16	56090.0
	4	- 1.227990	1.926850e-3	- 2.437050e-7	1.219300e-11	- 1.991840e-16	56090.0
	5	15.52020	- 3.885790e-3	3.228840e-7	- 9.605270e-12	9.547220e-17	56090.0
O	1	2.946428	- 1.638166e-3	2.421031e-6	- 1.602843e-9	3.890696e-13	29147.6
	2	2.542059	- 2.755061e-5	- 3.102803e-9	4.551067e-12	- 4.368051e-16	29230.8
	3	2.548	- 5.952e-5	2.701e-8	- 2.798e-12	9.380e-17	29150.0
	4	- 9.787120e-3	1.244970e-3	- 1.615440e-7	8.037990e-12	- 1.262400e-16	29150.0
	5	16.42810	- 3.931300e-3	2.983990e-7	- 8.161280e-12	7.500430e-17	29150.0

In McBride and Gordon's report, specific total enthalpy of species and specific heat in constant pressure of species are defined as,

$$\frac{h_s\left(T,T_V\right)}{RT} = -a_{1s}\frac{1}{T^2} + a_{2s}\frac{\ln(T)}{T} + a_{3s} + a_{4s}\frac{T}{2} + a_{5s}\frac{T^2}{3} + a_{6s}\frac{T^3}{4} + a_{7s}\frac{T^4}{5} + b_{1s}\frac{1}{T} \quad (23)$$

$$\frac{c_p^s}{R} = a_{1s}\frac{1}{T^2} + a_{2s}\frac{1}{T} + a_{3s} + a_{4s}T + a_{5s}T^2 + a_{6s}T^3 + a_{7s}T^4 \quad (24)$$

Parameters of the curve fit are obtained from their report. For example, the parameters of N2, N, and O are as listed in Tables 4 to 6.

Table 4. Curve fit parameters for N2 in MaBride & Gordon's report

Parameter	200 – 1000 K	1000 – 6000 K	6000 – 20000 K
a_{1s}	2.210371497×10^{4}	5.877124060×10^{5}	8.31013916×10^{8}
a_{2s}	-3.818461820×10^{2}	-2.239249073×10^{3}	-6.42073354×10^{5}
a_{3s}	6.082738360	6.066949220	2.020264635×10^{2}
a_{4s}	$-8.530914410\times10^{-3}$	$-6.139685500\times10^{-4}$	$-3.065092046\times10^{-2}$
a_{5s}	1.384646189×10^{-5}	1.491806679×10^{-7}	2.486903333×10^{-6}
a_{6s}	$-9.625793620\times10^{-9}$	$-1.923105485\times10^{-11}$	$-9.705954110\times10^{-11}$
a_{7s}	$2.519705809\times10^{-12}$	$1.061954386\times10^{-15}$	$1.437538881\times10^{-15}$
b_{1s}	7.108460860×10^{2}	1.283210415×10^{4}	4.938707040×10^{6}

Table 5. Curve fit parameters for N in MaBride & Gordon's report

Parameter	200 – 1000 K	1000 – 6000 K	6000 – 20000 K
a_{1s}	2.5	8.876501380×10^{4}	5.475181050×10^{8}
a_{2s}	0	-1.071231500×10^{2}	-3.107574980×10^{5}
a_{3s}	0	2.362188287	6.91678274×10^{1}
a_{4s}	0	2.916720081×10^{-4}	$-6.847988130\times10^{-3}$
a_{5s}	0	$-1.729515100\times10^{-7}$	3.827572400×10^{-7}
a_{6s}	0	$4.012657880\times10^{-11}$	$-1.098367709\times10^{-11}$
a_{7s}	0	$-2.677227571\times10^{-15}$	$1.277986024\times10^{-16}$
b_{1s}	5.610463780×10^{4}	5.697351330×10^{4}	2.550585618×10^{6}

Table 6. Curve fit parameters for O in MaBride & Gordon's report

Parameter	200 – 1000 K	1000 – 6000 K	6000 – 20000 K
a_{1s}	-7.953611300×10^{3}	2.619020262×10^{5}	1.779004264×10^{8}
a_{2s}	1.607177787×10^{2}	-7.298722030×10^{2}	-1.082328257×10^{5}
a_{3s}	1.966226438	3.317177270	2.810778365×10^{1}
a_{4s}	1.013670310×10^{-3}	$-4.281334360\times10^{-4}$	-2.97532262×10^{-3}
a_{5s}	$-1.110415423\times10^{-6}$	1.036104594×10^{-7}	1.854997534×10^{-7}
a_{6s}	$6.517507500\times10^{-10}$	$-9.438304330\times10^{-12}$	$-9.438304330\times10^{-12}$
a_{7s}	$-1.584779251\times10^{-13}$	$2.725038297\times10^{-16}$	$2.725038297\times10^{-16}$
b_{1s}	2.840362437×10^{4}	3.392428060×10^{4}	8.89094263×10^{5}

Comparisons of vibration and electron energy (E_V) and its corresponding specific heat in constant volume (c_V) for N2, N, and O are shown in figs. 1 to 3.

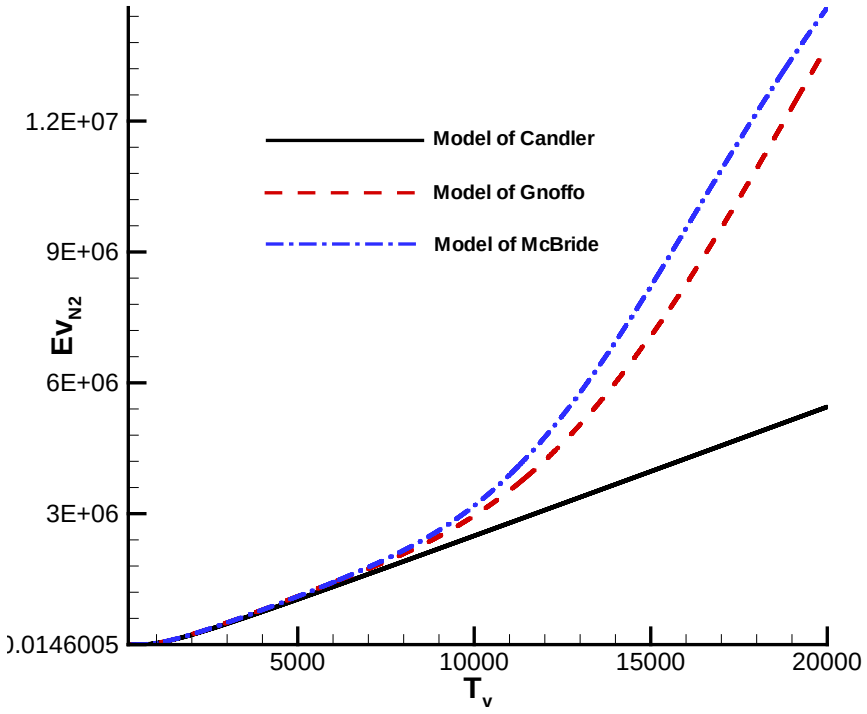

a)

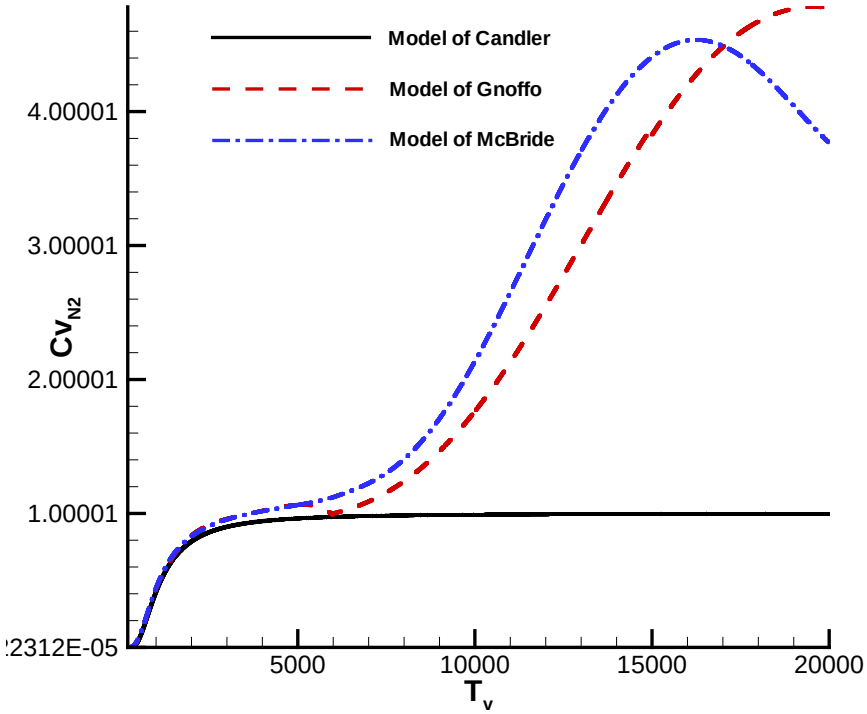

b)

Figure 1. vibration & electron energy and corresponding specific heat in constant volume of N2

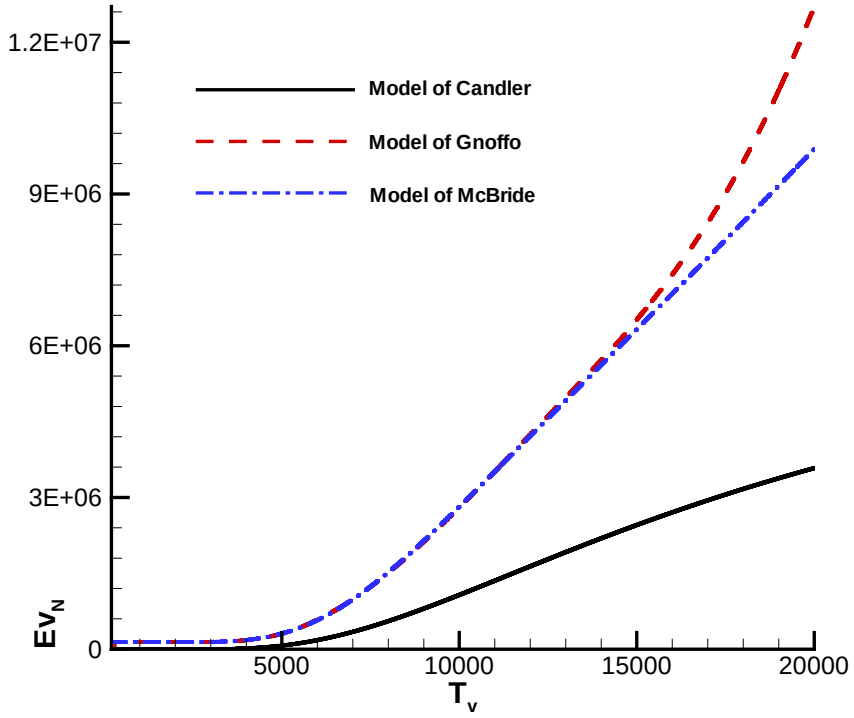

a)

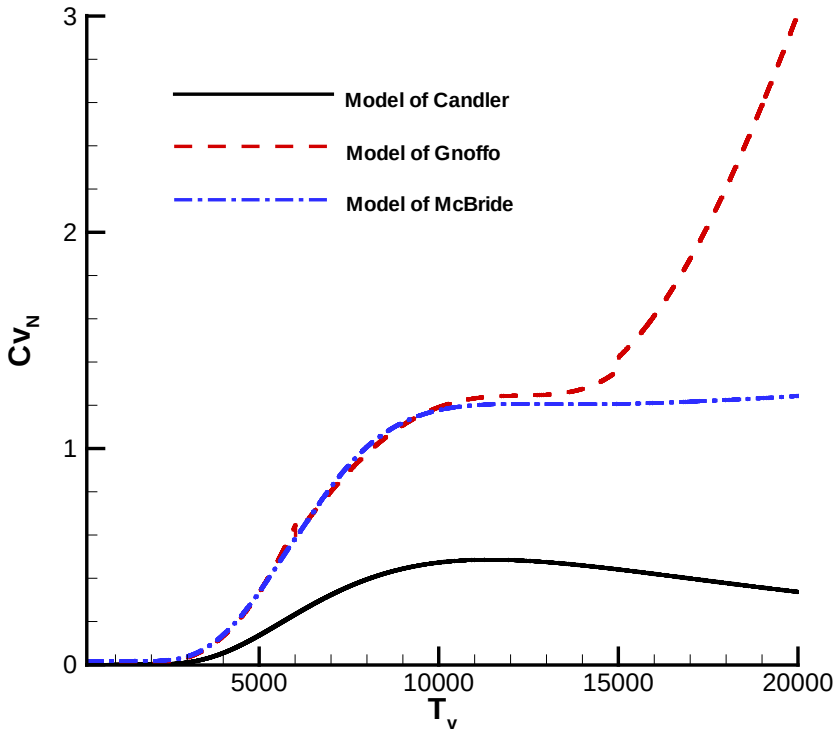

b)

Figure 2. vibration & electron energy and corresponding specific heat in constant volume of N

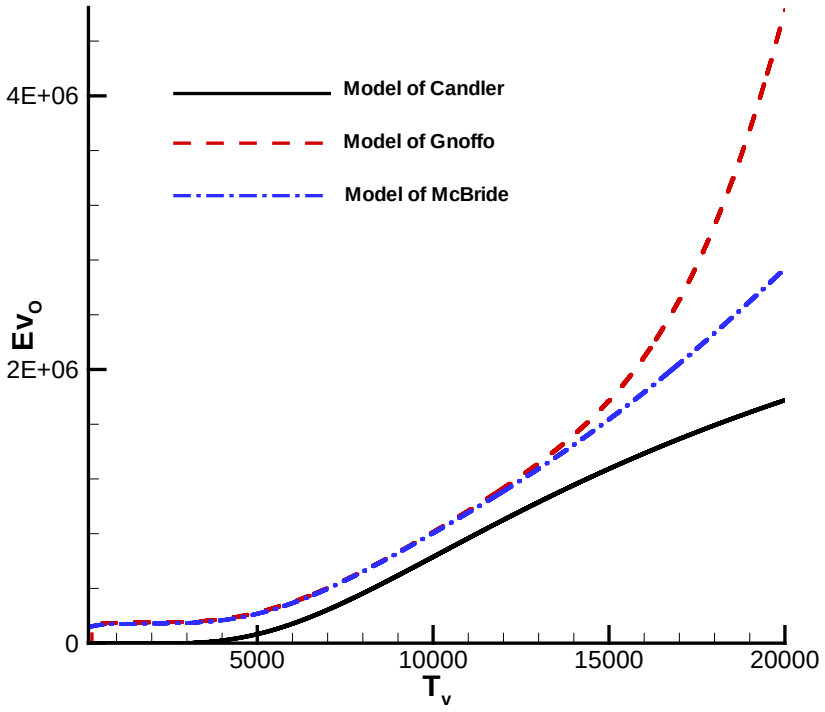

a)

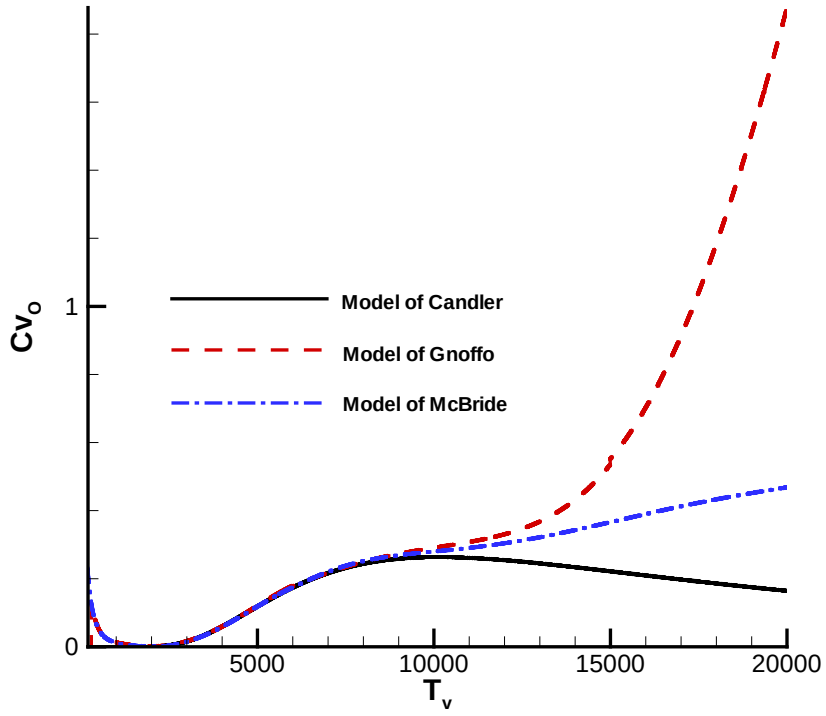

b)

Figure 3. vibration & electron energy and corresponding specific heat in constant volume of O

Figures 1 to 3 show that electron energy mode is quite significant when the vibration temperature increase to around 5,000 K.

4.2 Thermal properties

The viscosity of each species is calculated from the following curve fits. For the five species considered in current code, coefficients of curve fits are listed in Table 7, with the original data being obtained from Candler's dissertation [18].

$$\mu_s = 0.1\exp\left[(A_s \ln T + B_s)\ln T + C_s\right] \tag{25}$$

Table 7. Curve fit coefficients of 5-species viscosity

Species	N2	O2	NO	N	O
A_s	0.0268142	0.0449290	0.0436378	0.0115572	0.0203144
B_s	0.3177838	-0.0826158	-0.0335511	0.6031679	0.4294404
C_s	-11.3155513	-9.2019475	-9.5767430	-12.4327495	-11.6031403

By combining the viscosity of each species, the total viscosity is calculated as

$$\mu = \sum_{s=1}^{5} \frac{y_s \mu_s}{\phi_s} \tag{26}$$

Heat conductivities of each species corresponding to translation temperature and vibration temperature are calculated as

$$\kappa_s = \mu_s\left(\frac{5}{2}c_{vtr,s} + c_{vrot,s}\right) \tag{27}$$

$$\kappa_{Vs} = \mu_s c_V \tag{28}$$

Total heat conductivities are calculated from species heat conductivities in a way similar to calculating total viscosity from species viscosities,

$$\kappa = \sum_{s=1}^{5} \frac{y_s \kappa_s}{\phi_s} \tag{29}$$

$$\kappa_V = \sum_{s=1}^{5} \frac{y_s \kappa_{Vs}}{\phi_s} \tag{30}$$

In equations (26) to (30),

$$\phi_s = \sum_r y_r \left[1 + \sqrt{\frac{\mu_s}{\mu_r}}\left(\frac{M_r}{M_s}\right)^{1/4}\right]^2 \left[\sqrt{8\left(1+\frac{M_s}{M_r}\right)}\right]^{-1}$$

The diffusion coefficient is determined by assuming a constant Lewis number,

$$D_s = \frac{\kappa L_e}{\rho c_p} \text{(Neutral heavy species, } L_e = 1.4) \tag{31}$$

For 11-species air, a more complex model of thermal properties is applied [21]. According to this model, thermal properties are calculated as follows,

$$\mu = \sum_{s \neq e} \frac{m_s \gamma_s}{\sum_{r \neq e} \gamma_r \Delta_{sr}^{(2)}(T) + \gamma_e \Delta_{se}^{(2)}(T_V)} + \frac{m_e \gamma_e}{\sum \gamma_r \Delta_{er}^{(2)}(T_V)} \quad \textbf{(g/cm-sec)} \qquad (32)$$

$$K_T = \frac{15}{4} k \sum_{s \neq e} \frac{\gamma_s}{\sum_{r \neq e} a_{sr} \gamma_r \Delta_{sr}^{(2)}(T) + 3.54 \gamma_e \Delta_{se}^{(2)}(T_V)} \quad \textbf{(J/cm-sec-K)} \qquad (33)$$

In above equation, $a_{sr} = 1 + \dfrac{\left[1 - (m_s/m_r)\right]\left[0.45 - 2.54(m_s/m_r)\right]}{\left[1 + (m_s/m_r)\right]^2}$

$$K_R = k \sum_{s=mol} \frac{\gamma_s}{\sum_{r \neq e} \gamma_r \Delta_{sr}^{(1)}(T) + \gamma_e \Delta_{se}^{(1)}(T_V)} \quad \textbf{(J/cm-sec-K)} \qquad (34)$$

$$K_{V-E} = k \frac{C_{V,V}}{R} \sum_{s=1}^{11} \frac{\gamma_s}{\sum_{r \neq e} \gamma_r \Delta_{sr}^{(1)}(T) + \gamma_e \Delta_{se}^{(1)}(T_V)} \quad \textbf{(J/cm-sec-K)} \qquad (35)$$

$$K_e = \frac{15}{4} k \frac{\gamma_e}{\sum_{r \neq e} 1.45 \gamma_r \Delta_{er}^{(2)}(T_V) + \gamma_e \Delta_{ee}^{(2)}(T_V)} \quad \textbf{(J/cm-sec-K)} \qquad (36)$$

To calculate viscosity and heat conductivity, from equation (32) to equation (36), the collision terms are as follows,

$$\Delta_{sr}^{(1)}(T) = \frac{8}{3}\left[\frac{2 m_s m_r}{\pi R T (m_s + m_r)}\right]^{1/2} 1 \; \bar{0}^{20} \pi \Omega_{sr}^{(1,1)}(T) \quad \textbf{(cm-sec)}$$

$$\Delta_{sr}^{(2)}(T) = \frac{16}{3}\left[\frac{2 m_s m_r}{\pi R T (m_s + m_r)}\right]^{1/2} 1 \; \bar{0}^{20} \pi \Omega_{sr}^{(2,2)}(T) \quad \textbf{(cm-sec)}$$

Collision integrals involving neutrals (Non-Coulombic collision integrals) are

$$\pi \Omega_{sr}^{(l,j)}(T) = D T^{\left[A(\ln T)^2 + B \ln T + C\right]} \; (\overset{0}{\mathrm{A}}^2) \qquad (37)$$

The coulombic collision integrals for electron-ion, ion-ion, and electron-electron collision are computed as

$$\pi \Omega^{(l,l)}(T) = 5.0 \times 10^{15} \pi \left(\lambda_D / T^*\right)^2 \ln\left\{D_l T^* \left[1 - C_l \exp(-c_l T^*)\right] + 1\right\} \; (\overset{0}{\mathrm{A}}^2) \qquad (38)$$

where

$$T^* = \frac{\lambda_D}{e^2/(kT)} \qquad \lambda_D = \sqrt{\frac{kT}{4\pi N_e e^2}}$$

Species diffusion coefficients are defined as,

$$D_s = \frac{(1-y_s)}{\sum_{r\neq s}\left(y_r / D_{sr}\right)} \tag{39}$$

where y_s is the molar fraction. For binary diffusion between heavy particles,

$$D_{sr} = \frac{kT}{p\Delta_{sr}^{(1)}(T)}$$

For electrons,

$$D_{er} = \frac{kT_V}{p\Delta_{er}^{(1)}(T_V)}$$

For ambipolar diffusion (no charge separation), we have,

$$D_{ion}^a = 2D_{ion} \qquad D_e = M_e \frac{\sum_{s=6}^{10} D_s^a \gamma_s}{\sum_{s=6}^{10} M_s \gamma_s}$$

4.3 Chemical source terms

The forward and backward reaction rate coefficients have the form of

$$k_f\left(\overline{T}\right) = C_f \overline{T}^{\eta_f} \exp\left(-\theta_f / \overline{T}\right) \tag{40}$$

$$k_b\left(T\right) = \frac{k_f(T)}{k_{eq}(T)} \tag{41}$$

For dissociation reactions, $\overline{T} = \sqrt{TT_V}$. For electron impact ionization reactions, the control temperature is T_V. For the other reactions, the control temperature is T.

The equilibrium constant is calculated from the free Gibbs energy,

$$\ln k_{eq} = -\frac{\Delta_f G^0}{\overline{R}T} \tag{42}$$

where $\Delta_f G^0$ is the reaction standard Gibbs energy, which is the sum of the standard Gibbs energies of the reaction products minus the sum of standard Gibbs energies of reactants,

$$\ln k_{eq} = \sum_{s=reactant}\left(\frac{h_s}{RT} - \frac{S_s}{R}\right) - \sum_{s=product}\left(\frac{h_s}{RT} - \frac{S_s}{R}\right) \tag{43}$$

Table 7. chemistry of 11-species air and parameters of reaction rate

Index	Reaction	C_f (m^3/kmol-s)	η_f	θ_f (K)
1	$N_2+M\leftrightarrow N+N+M$ $(M=N_2,O_2,NO)$ $N_2+M\leftrightarrow N+N+M\ (M=N,O)$	7.0D+18 3.0D+19	-1.60 -1.60	113200 113200
2	$O_2+M\leftrightarrow O+O+M$ $(M=N_2,O_2,NO)$ $O_2+M\leftrightarrow O+O+M\ (M=N,O)$	2.0D+18 1.0D+19	-1.50 -1.50	59360 59360
3	$NO+M\leftrightarrow N+O+M$ $(M=N_2,O_2,NO)$ $NO+M\leftrightarrow N+O+M\ (M=N,O)$	5.2D+12 1.1D+14	0.00 0.00	75500 75500
4	$N_2+O\leftrightarrow NO+N$	5.7D+9	0.42	42938
5	$NO+O\leftrightarrow O_2+N$	8.4D+9	0.00	19400
6	$N_2+e\leftrightarrow N+N+e$	3.0D+21	-1.60	113200
7	$N+e\leftrightarrow N^++e+e$	2.5D+31	-3.82	168600
8	$O+e\leftrightarrow O^++e+e$	3.9D+30	-3.78	158500
9	$N+O\leftrightarrow NO^++e$	5.3D+9	0.00	31900
10	$N+N\leftrightarrow N_2^++e$	4.4D+4	1.50	67500
11	$O+O\leftrightarrow O_2^++e$	7.1D-1	2.70	80600
12	$O^++N_2\leftrightarrow N_2^++O$	9.1D+8	0.36	22800
13	$O^++NO\leftrightarrow N^++O_2$	1.4D+2	1.90	26600
14	$NO^++O_2\leftrightarrow O_2^++NO$	2.4D+10	0.41	32600
15	$NO^++N\leftrightarrow N_2^++O$	7.2D+10	0.00	35500
16	$NO^++O\leftrightarrow N^++O_2$	1.0D+9	0.50	77200
17	$O_2^++N\leftrightarrow N^++O_2$	8.7D+10	0.14	28600
18	$O_2^++N_2\leftrightarrow N_2^++O_2$	9.9D+9	0.00	40700
19	$NO^++N\leftrightarrow O^++N_2$	3.4D+10	-1.08	12800
20	$NO^++O\leftrightarrow O_2^++N$	7.2D+9	0.29	48600
21	$O_2^++O\leftrightarrow O^++O_2$	4.0D+9	-0.09	18000
22	$N^++N_2\leftrightarrow N_2^++N$	1.0D+9	0.50	12200

4.4 Energy relaxation

In two temperature model, energy relaxation only happens between translation energy and vibration & electron energy, which can be expressed as

$$Q_{T-v,s} = \rho_s \frac{e_{vs}^*(T) - e_{vs}}{\tau_{vs}} \tag{44}$$

where, $e_{vs}^*(T)$ is the vibration energy per unit mass of species s evaluated at the local translational temperature.

$$\tau_{vs} = \left\langle \tau_{s,L-T} \right\rangle + \tau_{cs} = \frac{\sum_r y_r}{\sum_r y_r / \tau_{sr,L-T}} + \frac{1}{a_s \sigma_v N_s} \qquad (a_s = \sqrt{\frac{8\bar{R}T}{\pi M_s}})$$

$$\tau_{sr,L-T} = \frac{1}{p} \exp\left[A_{sr} \left(T^{-1/3} - 0.015 \mu_{sr}^{1/4} \right) - 18.42 \right] \text{ (p in atm)}$$

$$A_r = 1.16 \times 10^{-3} \mu_{sr}^{1/2} \theta_{vs}^{4/3} \qquad \mu_{sr} = M_s M_r / (M_s + M_r)$$

$$S_s = 3.5 \exp\left(-\theta_s / T_{shk} \right) \qquad \sigma_v = 10^{-21} \left(50,000 / T \right)^2$$

Here, θ_s is a defined characteristic temperature.

The translation-electron relaxation is obtained as follows,

$$Q_{T-e} = 3R\rho_e (T - T_V) \sqrt{\frac{8RT_V}{\pi M_e}} \sum_{s=1}^{10} \frac{\rho_r \hat{N}}{M_r^2} \sigma_{er} \tag{45}$$

The formula of the cross-section is,

$$\sigma_{er} = \begin{cases} \bar{a}_r + \bar{b}_r T_V + \bar{c}_r T_V^2 & (electron - neutral) \\ \dfrac{8\pi}{27} \dfrac{e^4}{k^2 T_V^2} \ln\left(1 + \dfrac{9k^3 T_V^3}{4\pi N_e e^6}\right) & (electron - ions) \end{cases}$$

5. Validation resutls

The new code has been tested for two- and three-dimensional problems. We now start implementing the high-order shock-capturing filtering method so that the strong shock-turbulence interaction can be accurately solved.

5.1 Lobb's air flow over a sphere

In this case, the flow over a sphere corresponding to Lobb's experiment [22] is tested. The same flow has been numerically studied by Candler et al. [18]. Both five-species

model and eleven-species model of air are used. Our numerical simulation results are compared with both Lobb's experimental measurement and Candler's numerical results.

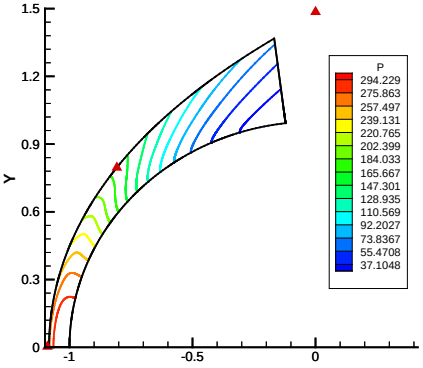

Figure 4. Comparison with Lobb's experiment: shock standoff distance

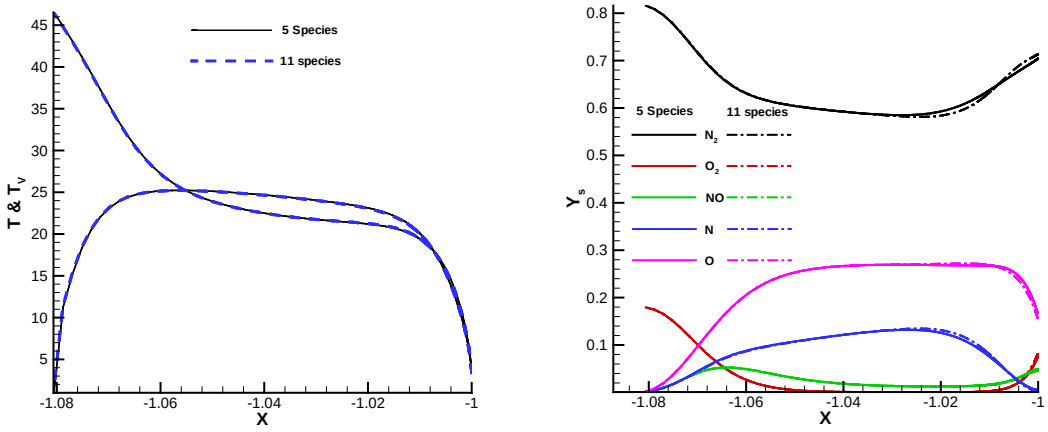

(a) (b)

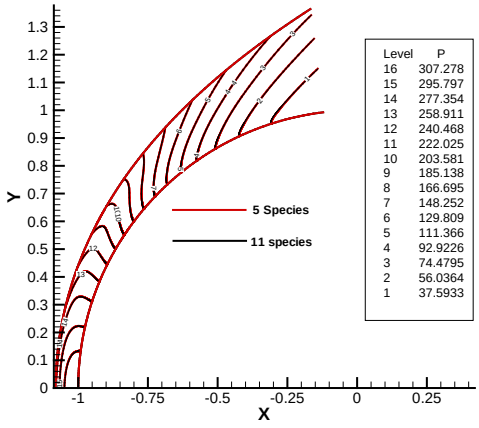

(c)

Figure 5. Comparisons of 5-species model and 11-species model: (a) temperatures along stagnation line; (b) mole fraction along the stagnation line; (c) pressure contour.

Figure 4 shows that shock standoff distance obtained from our numerical simulations has a very good agreement with the experimental measurement of Lobb, which also indicates that the non-equilibrium models are accurately implemented to the high-order shock-fitting method. Numerical simulation results obtained from five-species air model and eleven-species model respectively are compared in Fig. 5. It is notice that, for current case, there is no major difference between the two air models, because the temperature of this case is not high enough so that the ionizations of air species are still weak. We will further test our code by running cases with much higher temperature. For this case, we also compute the flow field over a cylinder under the same flow condition. The distribution of species densities along the stagnation line of 2-D simulation (cylinder) is compared with that of 3-D simulation (sphere) in Fig. 6. It is clearly shown that the shock standoff distance of 2-D simulation is much larger than that of 3-D simulation, although the species density distributions have similar profile.

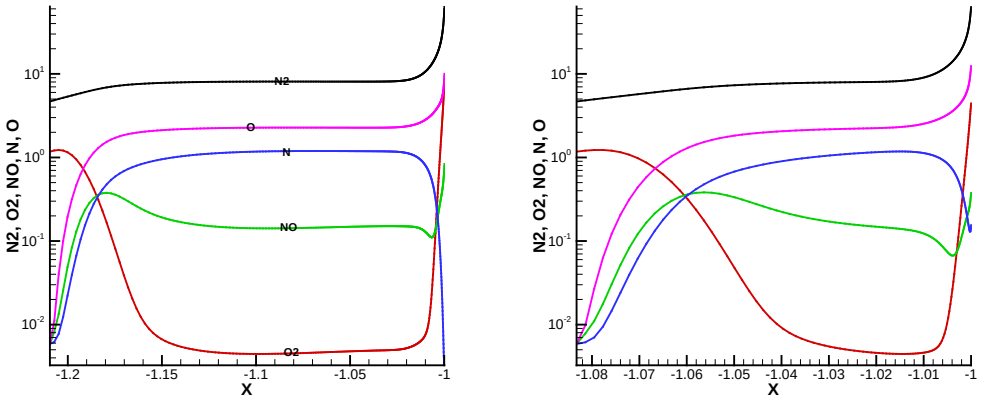

Figure 6. Comparisons of 2-D cylinder and 3-D sphere results under the same flow condition: species densities along the stagnation line.

5.2 Gnoffo's air flow over 1 m radius cylinder

The isothermal boundary conditions on the cylinder currently used are as follows,

$\frac{\partial c_s}{\partial \eta} = 0$, where c_s is mass fraction $\qquad \frac{\partial p}{\partial \eta} = 0$

u = v = w = 0, no-slip condition

The temperatures on the cylinder are equal to T_w (= 500 K). Total density is computed from pressure and translational temperature. Then species densities are calculated with total density and mass fraction. Total energy and vibration energy are calculated using species densities and two temperatures. The mass fractions of initial gas are as follows,

$C_{N2} = 0.76$, $C_{O2} = 0.24$

$C_{NO} = C_N = C_O = 0$

To make the results comparable, all simulations are carried out on a 61 × 129 grid, exactly the same as what Gnoffo used in his simulation. Flow conditions and geometry are schematically shown below. The simulation results are compared with Gnoffo's results obtained from Laura.

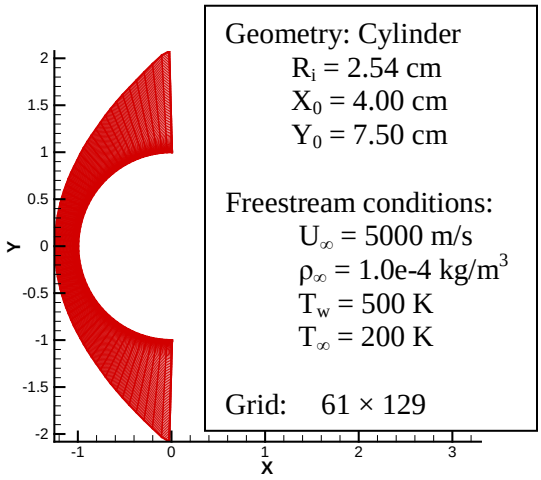

Figure 7. Geometry and free stream flow conditions.

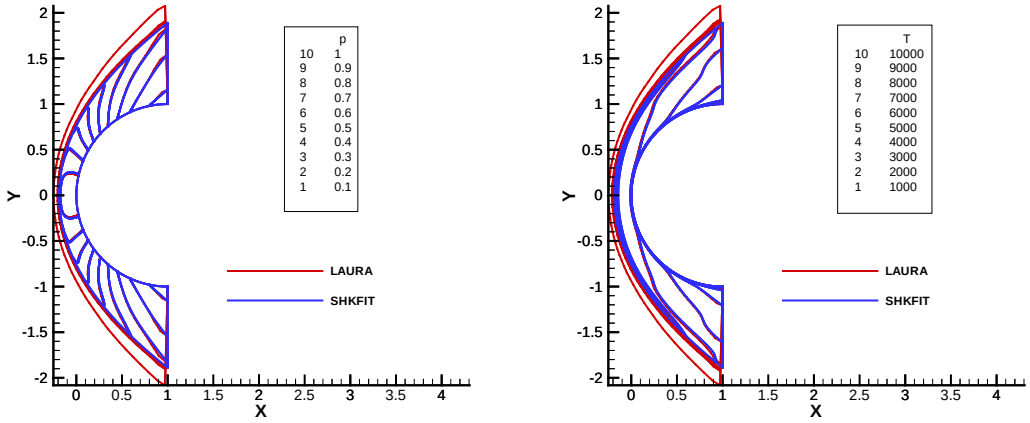

(a) (b)

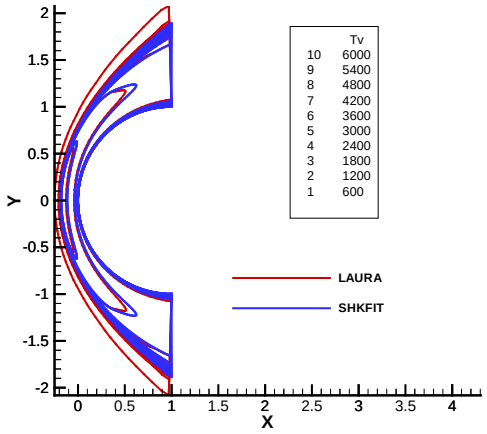

(c)

Figure 8. Comparisons of flow field obtained from shock-fitting method with Gnoffo's results: (a) pressure contour, (b) translation temperature contour, (c) vibration temperature contour.

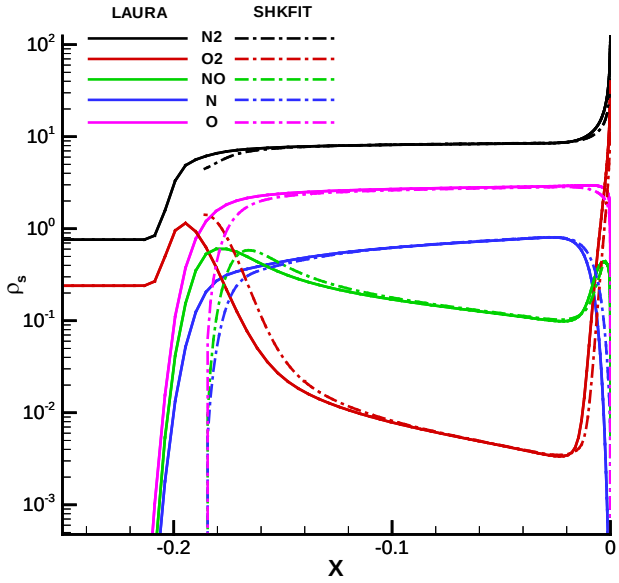

Figure 9. Comparisons of species densities along the stagnation line obtained from shock-fitting method with Gnoffo's results.

Figure 8 compares flow field obtained from shock-fitting method with Gnoffo's results. The comparisons of pressure and temperature contours show that the numerical results obtained from the new implemented shock-fitting method have a good agreement with Gnoffo's results. The shock standoff distance is almost the same. Figure 9 compares species densities along the stagnation line obtained from shock-fitting method with Gnoffo's results. Except the difference near the shock, species densities have a good agreement along the stagnation line. Near the shock, the difference of species densities comes from the different treatment of the shock.

6. Summary

In this paper, a high-order shock-fitting non-equilibrium flow solver is developed. The code is implemented based on a two-temperature model. It is assumed that translational and rotational energy modes are in equilibrium at the translational temperature whereas vibration energy, electronic energy, and free electron energy are in equilibrium at the vibration temperature. In the computer code, both 5-species and 11-species chemistry sets of air are implemented. The flow solver uses fifth-order shock-fitting method of Zhong [17]. For the inviscid flux vectors, a simple local Lax-Friedrichs scheme is used to split vectors into negative and positive wave fields. The inviscid flux terms are discretized by a fifth-order upwind scheme, and the viscous flux terms are discretized by a sixth-order central scheme. The conditions behind the shock are calculated using Rankine-Hugoniot relations across the shock, a compatibility relation from behind the shock, and the same species concentration across the shock. The code is being tested on a number of non-equilibrium reacting flows. The results obtained from the new implemented shock-fitting code have a good agreement with experimental datasets and numerical simulation results

obtained from open literature. The high-order shock-fitting solver will be applied to numerical simulations of strong shock and turbulence interaction, and hypersonic boundary-layer stability and transition problems.

Acknowledgement

The research was supported partially by DOE office of Science as part of a SciDAC project with "Science Application" in Turbulence and partially by the AFOSR/NASA National Center for Hypersonic Research in Laminar-Turbulent Transition. The authors appreciate Dr. Peter A. Gnoffo's help on running the 5-species air over 1 meter radius cylinder using LAURA code. This test cases are mainly run on TeraGrid resources provided by TACC under grant number TG-ASC100002 supported in part by the National Science Foundation. The views and conclusions contained herein are those of the authors and should not be interpreted as necessarily representing the official policies or endorsements either expressed or implied, of the Air Force Office of Scientific Research or the U.S. Government.

Reference

1. Anderson Jr., J.D., *Hypersonic and High Temperature Gas Dynamics*. 1998: McGraw-Hill.
2. Rawat, P.S., and Zhong, X., *On High-Order Shock-Fitting and Front-Tracking Schemes for Numerical Simulation of Shock-Disturbance Interactions.* Journal of Computational Physics, 2010. **229**(19): p. 6744-6780.
3. Rawat, P.S., and Zhong, X., *Simulation of Strong Shock and Turbulence Interactions using High-Order Shock-Fitting Algorithms.* Bulletin of the American Physical Society, 2010. **55(16)**
4. Lele, S.K., and Larsson, J., *Shock-turbulence interaction: What we know and what we can learn from peta-scale simulations.* Journal of Physics: Conference Series, 2009. **180**(012032).
5. Wang, X., and Zhong, X., *Receptivity of a Mach 8 Flow over a Sharp Wedge to Wall Blowing-Suction.* 2005. **AIAA paper 2005-5025**.
6. Wang, X., and Zhong, X., *Numerical Simulation and Experiment Comparison of Leading-Edge Receptivity of a Mach 5.92 Boundary Layer.* AIAA paper 2006-1107, 2006.
7. Wang, X., and Zhong, X., *Effect of wall perturbations on the receptivity of a hypersonic boundary layer.* Physics of fluids, 2009. **21** (044101).
8. Vincenti, W.G., and Kruger Jr., C. H., *Introduction to Physical Gas Dynamics* 1967: Krieger Publishing Co, INC.
9. Mannella, G.G., *Chemical Reactions in Electrical Plasmas.* The OHIO Journal of Science, 1966. **66**(3): p. 334-339.
10. Wright, M.J., Olejniczak, J., Walpot, L., Raynaud, E., Magin, T., Caillaut, L, and Hollis, B. R. , *A Code Calibration Study for Huygens Entry Aeroheating*. 2006, AIAA 2006-0382.

11. Gnoffo, P.A., Mccandless, R. S., and Yee, H. C., *Enhancements to Program LAURA for Computation of Three-Dimensional Hypersonic Flow* 1987, AIAA 1987-0280.
12. Gnoffo, P.A., *Computational Aerothermodynamics in Aeroassist Applications*. 2001, AIAA 2001-2623.
13. Gnoffo, P.A., *Computational Fluid Dynamics Technology for Hypersonic Applications*. 2003, AIAA 2003-3259.
14. Hash, D., Olejniczak, J, Wright, M. J., Dinish, P., Pulsonetti, M., Hollis, B. R., Gnoffo, P. A., Barnhard, M., Nompelis, I., and Candler, G., *FIRE II Calculations for Hypersonic Nonequilibrium Aerothermodynamics Code Validation: DPLR, LAURA, and US3D*. 2007, AIAA 2007-0605.
15. Wright, M.J., Candler, G. V., and Bose, D., *Data-Parallel Line Relaxation Method for the Navier–Stokes Equations.* AIAA Journal, 1998. **36**(9): p. 1603-1609.
16. Walpot, L., *Development and Application of a Hypersonic Flow Solver*. 2002, T. U. Delft University.
17. Zhong, X., *High-order finite-difference schemes for numerical simulation of hypersonic boundary-layer transition.* Journal of Computational Physics, 1998. **144**: p. 662-709.
18. Candler, G.V., *The computation of weakly ionized hypersonic flows in thermo-chemical nonequilibrium*. 1988, Stanford University.
19. Gnoffo, P.A., Gupta, R. N., and Shinn, J. L., *Conservation equations and physical models for hypersonic air flows in thermal and chemical nonequilibrium*. 1989, NASA Technical Paper 2867.
20. McBride, B.J., and Gordon, S., *Fortran IV program for calculation of thermodynamic data*. 1967, NASA TN D-4097.
21. Gupta, R.N., Yos, J. M., Thompson, R. A., and Lee, K-P., *A Review of Reaction Rates and Thermodynamic and Transport Properties for an 11-Species Air Model for Chemical and Thermal Nonequilibrium Calculations to 30 000 K*. 1990, NASA Reference Publication 1232.
22. Lobb, R.K., *Experimental Measurement of Shock Detachment Distance on Spheres Fired in Air at Hypervelocities*, in *The High Temperature Aspects of Hypersonic Flow*, W.C. Nelson, Editor. 1964, MacMillan Co.: New York.